JOURNAL OF GUIDANCE, CONTROL, AND DYNAMICS
Vol. 33, No. 2, March–April 2010

Engineering Notes

Linear-Parameter-Varying Control of an Improved Three-Degree-of-Freedom Aeroelastic Model

Zebb Prime,* Ben Cazzolato,† and Con Doolan‡
University of Adelaide,
Adelaide, South Australia 5005, Australia
and
Thomas Strganac§
Texas A&M University, College Station, Texas 77843

DOI: 10.2514/1.45657

I. Introduction

AEROELASTICITY is a broad term that describes the often complex interactions between aerodynamics and structural mechanics. The active control of aeroelastic phenomena is of particular research interest, as it can lead to a reduction in weight and an increase in performance of an airframe. For more background on the analysis and control of aeroelastic systems, the reader is referred to Mukhopadhyay [1].

A two-degree-of-freedom wing section that is allowed to pitch and plunge due to supporting translational and torsional springs has often been used as a testbed for novel aeroelastic control methodologies. Two such apparatuses are commonly used for the experimental validation of these methodologies: the benchmark active control technologies wing [1,2] and the nonlinear aeroelastic test apparatus (NATA) [3,4].

This work focuses on the NATA platform and presents an improved dynamic model, a dynamicless state-feedback linear-parameter-varying (LPV) controller that self-schedules with airspeed U, and experimental results showing the suppression of limit-cycle oscillations.

Many practical and theoretical studies based on the NATA use the two-degree-of-freedom models as published in Platanitis and Strganac [4]. However, this model does not correctly model the inertia from the portion of the carriage that rotates and the control surface dynamics, which in this case are too slow to be neglected. The improved three-degree-of-freedom dynamic model presented in this work captures these effects and will benefit future theoretical and experimental research based on the NATA and similar platforms.

Using an $\mathcal{H}_2$ representation of the standard linear quadratic regulator (LQR) control problem, a state-feedback controller of the form $\mathbf{u} = \mathbf{K}(U)\mathbf{x}$ is synthesized using linear matrix inequalities (LMIs) as a generalized LPV control problem. This controller assumes that $\dot{U}$ is much slower than the airfoil dynamics and can be approximated as equal to zero and that, once stable, the torsional stiffness nonlinearity present in Strganac et al. [3] has little influence and hence can be approximated as $k_\alpha(\alpha) = k_\alpha$.

Received 26 May 2009; revision received 30 October 2009; accepted for publication 30 October 2009.

*Graduate Student, School of Mechanical Engineering; zebb.prime@adelaide.edu.au.

†Associate Professor, School of Mechanical Engineering.

‡Senior Lecturer, School of Mechanical Engineering. Senior Member AIAA.

§Professor, Department of Aerospace Engineering. Associate Fellow AIAA.

II. Model

Consider the typical section airfoil shown in Fig. 1, with three degrees of freedom: pitch α, plunge h, and trailing-edge surface deflection β. The wing section is forced by an aerodynamic lift force L and moment M coupled to the freestream conditions and the dynamic state of the airfoil.

The wing section is divided into three distinct bodies: a translational body of mass m_h, which corresponds to the nonrotational component of the carriage in the experimental apparatus (Sec. III); the rotational wing body of mass m_α and inertia I_α, which corresponds to the main wing body plus the rotational component of the carriage in the experimental apparatus; and the rotational trailing-edge section of mass m_β and inertia I_β. The trailing-edge servo motor provides a torque between the wing body and the trailing-edge section. These bodies, and their associated reference frames, are shown in Fig. 1.

The equations of motion are derived using a Lagrangian energy method. The Lagrangian, the difference between the kinetic and potential energies, is

$$\mathcal{L} = (T_1 + T_2 + T_3) - (V_1 + V_2 + V_3) \tag{1}$$

where T_i and V_i are the kinetic and potential energies of the ith frame. Assuming that the servo motor for the trailing edge can be modeled as a second-order system of the form

$$\ddot{\beta} + c_{\beta_{\text{servo}}}\dot{\beta} + k_{\beta_{\text{servo}}}\beta = k_{\beta_{\text{servo}}}\beta_{\text{des}} \tag{2}$$

(where $c_{\beta_{\text{servo}}}$ and $k_{\beta_{\text{servo}}}$ are the damping and stiffness, respectively, and $\beta_{\text{des.}}$ is the desired servo motor position), the full nonlinear equations of motion can be calculated as

$$\frac{\mathrm{d}}{\mathrm{d}t}\begin{bmatrix}\frac{\partial\mathcal{L}}{\partial\dot{h}}\\ \frac{\partial\mathcal{L}}{\partial\dot{\alpha}}\\ \frac{\partial\mathcal{L}}{\partial\dot{\beta}}\end{bmatrix} - \begin{bmatrix}\frac{\partial\mathcal{L}}{\partial h}\\ \frac{\partial\mathcal{L}}{\partial\alpha}\\ \frac{\partial\mathcal{L}}{\partial\beta}\end{bmatrix} = -\underbrace{\begin{bmatrix}0\\0\\k_{\beta_{\text{servo}}}\beta\end{bmatrix}}_{\text{forcing stiffness}} - \underbrace{\begin{bmatrix}c_h\dot{h}\\c_\alpha\dot{\alpha}\\c_{\beta_{\text{servo}}}\dot{\beta}\end{bmatrix}}_{\text{damping}} + \underbrace{\begin{bmatrix}-L\\M\\k_{\beta_{\text{servo}}}\beta_{\text{des}}\end{bmatrix}}_{\text{generalized forces}} \tag{3}$$

These nonlinear equations of motion are linearized using small-angle approximations for all of the trigonometric terms, which produces the linearized three-degree-of-freedom equation of motion:

$$\begin{bmatrix} m_h+m_\alpha+m_\beta & m_\alpha x_\alpha b+m_\beta r_\beta+m_\beta x_\beta & m_\beta r_\beta \\ m_\alpha x_\alpha b+m_\beta r_\beta+m_\beta x_\beta & \hat{I}_\alpha+\hat{I}_\beta+m_\beta x_\beta^2+2x_\beta m_\beta r_\beta & \hat{I}_\beta+x_\beta m_\beta r_\beta \\ m_\beta r_\beta & \hat{I}_\beta+x_\beta m_\beta r_\beta & \hat{I}_\beta \end{bmatrix} \times \begin{bmatrix}\ddot{h}\\ \ddot{\alpha}\\ \ddot{\beta}\end{bmatrix} + \begin{bmatrix} c_h & 0 & 0\\ 0 & c_\alpha & 0\\ 0 & 0 & c_{\beta_{\text{servo}}}\end{bmatrix}\begin{bmatrix}\dot{h}\\ \dot{\alpha}\\ \dot{\beta}\end{bmatrix} + \begin{bmatrix} k_h & 0 & 0\\ 0 & k_\alpha(\alpha) & 0\\ 0 & 0 & k_{\beta_{\text{servo}}}\end{bmatrix} \times \begin{bmatrix}h\\ \alpha\\ \beta\end{bmatrix} = \begin{bmatrix}-L\\ M\\ k_{\beta_{\text{servo}}}\beta_{\text{des}}\end{bmatrix} \tag{4}$$

where $k_\alpha(\alpha)$ and k_h are the pitch and plunge stiffness, respectively; c_α and c_h are the pitch and plunge viscous damping, respectively; $\hat{I}_\alpha = I_\alpha + m_\alpha x_\alpha^2 b^2$ is the moment of inertia of the wing about the elastic

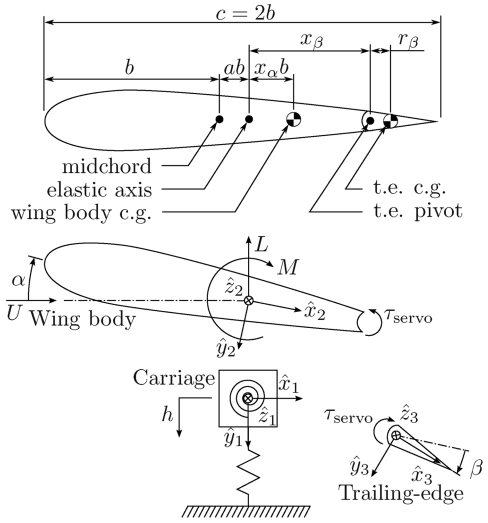

Fig. 1 Diagram of the aeroelastic system, including dimensions, loads, degrees of freedom, and reference frames used for the derivation of dynamics.

axis; and $\hat{I}_\beta = I_\beta + m_\beta r_\beta^2$ is the moment of inertia of the trailing edge about its pivot.

The aerodynamics of the wing are modeled using the quasi-steady aerodynamic model [3,4]:

$$L = \rho U^2 b S C_{l_\alpha}\left(\alpha + \frac{\dot{h}}{U} + \left(\frac{1}{2} - a\right) b\frac{\dot{\alpha}}{U}\right) + \rho U^2 b S C_{l_\beta}\beta \tag{5}$$

and

$$M = \rho U^2 b^2 S C_{m_{\alpha,\text{eff}}}\left(\alpha + \frac{\dot{h}}{U} + \left(\frac{1}{2} - a\right) b\frac{\dot{\alpha}}{U}\right) + \rho U^2 b^2 S C_{m_{\beta,\text{eff}}}\beta \tag{6}$$

where ρ is the freestream air density; S is the airfoil span; $C_{l_\alpha} = \partial C_l/\partial\alpha$ and $C_{l_\beta} = \partial C_l/\partial\beta$ are the pitch and trailing-edge deflection coefficients of lift, respectively; and

$$C_{m_{\alpha,\text{eff}}} = 2\frac{\partial C_m}{\partial\alpha} + \left(\frac{1}{2} + a\right) C_{l_\alpha} \tag{7}$$

and

$$C_{m_{\beta,\text{eff}}} = 2\frac{\partial C_m}{\partial\beta} + \left(\frac{1}{2} + a\right) C_{l_\beta} \tag{8}$$

This quasi-steady model is based on a steady aerodynamic model with additional linearized contributions to the angle of attack due to the pitching and plunging motion of the wing. This model describes the unsteady aerodynamics accurately for values of the Strouhal number, $f^* b/U < 0.1$, where f is the oscillation frequency of the airfoil.

The aeroelastic equations of motion can be found by substituting the quasi-steady aerodynamics (5) and (6) into the mechanical equations of motion (4) and rearranging the dynamic-state-dependent aerodynamic terms ($\alpha, \dot{\alpha}$, and $\dot{h}$) to the left-hand side. The aeroelastic equations of motion can then be converted to a state-space form by letting the state-vector be

$$\mathbf{x} = [\,\dot{h} \quad \dot{\alpha} \quad \dot{\beta} \quad h \quad \alpha \quad \beta\,]^T \tag{9}$$

with input $\mathbf{u} = \beta_{\text{des}}$ and output $\mathbf{y}$. This yields the LPV form

$$\begin{bmatrix}\dot{\mathbf{x}}\\ \mathbf{y}\end{bmatrix} = \begin{bmatrix}\mathbf{A}(U,\alpha) & \mathbf{B}\\ \mathbf{C} & \mathbf{D}\end{bmatrix}\begin{bmatrix}\mathbf{x}\\ \mathbf{u}\end{bmatrix} \tag{10}$$

where the parameter dependence of $\mathbf{A}$ takes the form

$$\mathbf{A}(U,\alpha) = \mathbf{A}_0 + \mathbf{A}_1 U + \mathbf{A}_2 U^2 + \mathbf{A}_3 k_\alpha(\alpha) \tag{11}$$

The output $\mathbf{y}$, and hence the $\mathbf{C}$ and $\mathbf{D}$ matrices, depends upon the sensor configuration. $\mathbf{C} = \mathbf{I}$ and $\mathbf{D} = 0$ for state feedback $\mathbf{y} = \mathbf{x}$.

III. Nonlinear Aeroelastic Test Apparatus

The NATA is an experimental platform at the Texas A&M University for the testing of nonlinear aeroelastic theory. It consists of a rigid-wing section with trailing- and leading-edge actuators connected to a carriage that allows it to pitch and plunge. Photographs and a schematic of the wing and carriage mechanism can be found in Platanitis and Strganac [4]. This particular wing section has been used in several other experimental studies, including Platanitis and Strganac [4,5].

The wind tunnel has a 0.91×0.61 m working section, is temperature-regulated (which was set to 13°C for all experiments), and is capable of over 50 m/s; however, the experimental velocity was limited to 15 m/s to prevent possible damage to the NATA. The velocity was measured using a pitot tube connected to a pressure transducer.

Both control surfaces are actuated by Futuba S9402 RC servo motors, driven by a pulse-width-modulated (PWM) signal running at 50 Hz with a duty cycle between 0.05 and 0.1 (pulse high time between 1 and 2 ms). The position of the control surfaces as well as the pitching angle and plunge displacement are measured using U.S. Digital E2-1024-375-H optical encoders, which have dual 1024-pulse/rev channels. These servo motors and encoders were directly connected to the breakout board of a Humusoft MF624 multifunction control board inside a host computer. The PWM signal from the MF624 is generated by two 32-bit hardware timers, and the encoders are read in hardware in quadrature for a resolution of 4096 pulses/rev. The output from the pressure transducer, which is connected to the pitot tube, is connected to a 14-bit analog-to-digital converter on the MF624. The MF624 was controlled using The Mathworks Real-Time Windows Target and Simulink.

The parameters of the NATA were measured when possible and were estimated using a nonlinear gray-box system identification process when it was not possible to measure the parameter, and they are shown in Table 1.

In particular, the torsional stiffness was measured by applying varying loads and measuring the resulting pitch angle, and the trailing-edge servo motor was modeled by applying a chirp signal with a magnitude equal to the servo motors maximum deflection, measuring the output position using the encoder and fitting a second-order model to this data.

Table 1 System parameters for the 3-DOF NATA model

m_h	6.516 kg
m_α	6.700 kg
m_β	0.537 kg
$\hat{I}_\alpha$	0.126 kg · m^2
$\hat{I}_\beta$	1.00×10^{-5} kg · m^2
b	0.1905 m
a	−0.673
x_α	0.21
r_β	0
x_β	0.233 m
S	0.5945 m
c_h	27.43 N · s/m
c_α	0.215 Nm · s/rad
$c_{\beta_{\text{servo}}}$	4.182×10^{-4} Nm · s/rad
k_h	2844 N/m
$k_\alpha(\alpha)$	$25.55 - 103.19\alpha + 543.2\alpha^2$ Nm/rad
$k_{\beta_{\text{servo}}}$	7.6608×10^{-3} Nm/rad
C_{l_α}	6.757
$C_{m_{\alpha,\text{eff}}}$	−1.17
C_{l_β}	3.774
$C_{m_{\beta,\text{eff}}}$	−2.1

IV. LPV LQR Control

The standard LQR control problem can be represented as a minimization of the $\mathcal{H}_2$ norm from a unit white-noise input $\mathbf{w}$ to a performance output $\mathbf{z}$ for the linear time-invariant state system described by [6]

$$\dot{\mathbf{x}} = \mathbf{A}\mathbf{x} + \mathbf{B}\mathbf{u} + \mathbf{w} \tag{12}$$

$$\mathbf{z} = \begin{bmatrix} \mathbf{Q}^{\frac{1}{2}} & 0 \\ 0 & \mathbf{R}^{\frac{1}{2}} \end{bmatrix} \begin{bmatrix} \mathbf{x} \\ \mathbf{u} \end{bmatrix} \tag{13}$$

where $\mathbf{Q}$ and $\mathbf{R}$ are the state and input weightings, respectively.

This can be represented in the form of a generalized control problem:

$$\begin{bmatrix} \dot{\mathbf{x}} \\ \mathbf{z} \\ \mathbf{y} \end{bmatrix} = \begin{bmatrix} \mathbf{A} & \mathbf{B}_1 & \mathbf{B} \\ \mathbf{C}_1 & \mathbf{D}_1 & \mathbf{E}_1 \\ \mathbf{C} & \mathbf{F}_1 & 0 \end{bmatrix} \begin{bmatrix} \mathbf{x} \\ \mathbf{w} \\ \mathbf{u} \end{bmatrix} \tag{14}$$

with $\mathbf{B}_1 = \mathbf{I}$, $\mathbf{C}_1 = [\mathbf{Q}^{\frac{1}{2}} \quad 0]^T$, $\mathbf{D}_1 = [0 \quad 0]^T$, $\mathbf{E}_1 = [0 \quad \mathbf{R}^{\frac{1}{2}}]^T$, and $\mathbf{F}_1 = 0$.

Given a parameter vector p, the closed-loop linear-parameter-varying state-space form of the generalized control problem (14) under state feedback $\mathbf{C} = \mathbf{I}$ with feedback gain $\mathbf{K}(p)$ is

$$\mathcal{G}(p) := \begin{bmatrix} \mathcal{A}(p) & \mathcal{B}_1(p) \\ \mathcal{C}_1(p) & \mathcal{D}_1(p) \end{bmatrix} := \begin{bmatrix} \mathbf{A}(p) + \mathbf{B}(p)\mathbf{K}(p) & \mathbf{B}_1(p) \\ \mathbf{C}_1(p) + \mathbf{E}_1(p)\mathbf{K}(p) & \mathbf{D}_1(p) \end{bmatrix} \tag{15}$$

With the parameter-dependent Lyapunov variable $\mathcal{X}(p)$ and auxiliary parameter $\mathcal{Z}(p)$, the $\mathcal{H}_2$ norm of the closed-loop system (15) is $\|\mathcal{G}(p)\|_2^2 < \nu$ if the analysis LMIs [7]

$$\begin{bmatrix} \dot{\mathcal{X}}(p) + \mathcal{A}^T(p)\mathcal{X}(p) + \mathcal{X}(p)\mathcal{A}(p) & \mathcal{X}(p)\mathcal{B}_1(p) \\ \mathcal{B}_1^T(p)\mathcal{X}(p) & -\mathbf{I} \end{bmatrix} < 0$$

$$\begin{bmatrix} \mathcal{X}(p) & \mathcal{C}_1^T(p) \\ \mathcal{C}_1(p) & \mathcal{Z}(p) \end{bmatrix} > 0 \qquad \mathrm{Tr}(\mathcal{Z}(p)) < \nu \qquad \mathcal{D}_1 = 0 \tag{16}$$

are feasible.

A general procedure for transforming analysis LMIs such as those in Eq. (16) is presented by Scherer [8]. This procedure involves transforming the controller parameters and the Lyapunov matrix into a new set of variables that render the LMIs affine. For the state-feedback case, two matrix variables are introduced: a transformed Lyapunov variable $\mathbf{Y}$ and a transformed controller variable $\mathbf{M}$. Then applying the congruence transformation from Scherer [8] to Eq. (16), the synthesis LMIs are obtained:

$$\begin{bmatrix} -\dot{\mathbf{Y}}(p) + \tilde{\mathbf{A}}(p) + \tilde{\mathbf{A}}(p)^T & \tilde{\mathbf{B}}(p) \\ \tilde{\mathbf{B}}(p)^T & -\mathbf{I} \end{bmatrix} < 0$$

$$\begin{bmatrix} \mathbf{Y}(p) & \tilde{\mathbf{C}}(p)^T \\ \tilde{\mathbf{C}}(p) & \mathbf{Z}(p) \end{bmatrix} > 0 \qquad \mathrm{Tr}(\mathbf{Z}(p)) < \nu \qquad \tilde{\mathbf{D}} = 0 \tag{17}$$

where the new variables are

$$\begin{bmatrix} \tilde{\mathbf{A}}(p) & \tilde{\mathbf{B}}(p) \\ \tilde{\mathbf{C}}(p) & \tilde{\mathbf{D}}(p) \end{bmatrix} = \begin{bmatrix} \mathbf{A}(p)\mathbf{Y}(p) + \mathbf{B}(p)\mathbf{M}(p) & \mathbf{B}_1(p) \\ \mathbf{C}_1(p)\mathbf{Y}(p) + \mathbf{E}_1(p)\mathbf{M}(p) & \mathbf{D}_1(p) \end{bmatrix} \tag{18}$$

The synthesis LMIs are now affine in the variables $\mathbf{Y}(p)$ and $\mathbf{M}(p)$.

The controller gain and Lyapunov matrix can be calculated as $\mathcal{X}(p) = \mathbf{Y}^{-1}(p)$ and $\mathbf{K}(p) = \mathbf{M}(p)\mathbf{Y}^{-1}(p)$.

As shown in Eq. (10), the LPV state equation depends upon both the airspeed U and the pitching angle α. The dependence upon the pitching angle is a result of the torsional-spring stiffness nonlinearity, which increases with increasing pitch angle. This nonlinearity has a stabilizing influence, preventing the system from going unstable, instead putting it into limit-cycle oscillations. It has been argued [9] that this nonlinearity can be neglected when designing a stabilizing control law. Thus linearizing the torsional stiffness, the parameter-dependent state matrix takes the form

$$\mathbf{A}(U) = (\mathbf{A}_0 + \mathbf{A}_3 k_\alpha(0)) + \mathbf{A}_1 U + \mathbf{A}_2 U^2 \tag{19}$$

The parameter-dependent transformed controller variable and transformed Lyapunov variable are given the same form as Eq. (19):

$$\mathbf{Y}(U) = \mathbf{Y}_0 + \mathbf{Y}_1 U + \mathbf{Y}_2 U^2 \tag{20}$$

$$\mathbf{M}(U) = \mathbf{M}_0 + \mathbf{M}_1 U + \mathbf{M}_2 U^2 \tag{21}$$

The synthesis LMIs (17) in the matrix variables $\mathbf{Y}_i$ and $\mathbf{M}_i$ for $i = 0, 1, 2$ were constructed in MATLAB using the package Yalmip [10]. The parameters for the NATA given in Table 1 and the state and input weightings that were used are

$$\mathbf{Q} = \mathrm{diag}(1, 10, 1 \times 10^{-4}, 0.1, 1, 1 \times 10^{-4}) \tag{22}$$

$$\mathbf{R} = 100 \tag{23}$$

The LMIs were simultaneously solved using the SDPT3 [11] solver at 50 evenly spaced points between $U = 8$ and 40 m/s, as well as at points formed by the intersection of the tangents of U^2 such that 49 triangular grid regions were formed over the U-vs-U^2 curve. The solution yielded numerical values of $\mathbf{Y}_i$, $\mathbf{M}_i$, and ν, and the resulting performance index was $\nu = 108.5$. The resulting controller gains and performance index were verified on a finer grid spanning the same range, but containing 1000 evenly spaced grid points (999 triangular grid regions).

When the controller is reconstructed as $\mathbf{K}(U) = \mathbf{M}(U)\mathbf{Y}^{-1}(U)$, the controller gain $\mathbf{K}(U)$ is a high-order rational function of airspeed. This can be symbolically calculated offline, but the high order of the rational function as well as the poor numerical conditioning of the function parameters render this impractical. Instead, $\mathbf{K}(U)$ is numerically calculated online at each time step from $\mathbf{M}(U)$ and $\mathbf{Y}(U)$.

V. Results

The synthesized controller was tested on the NATA described in Sec. III. Though the controller was designed over the airspeed range $U \in [8 \quad 40]$ m/s, experiments were only performed up to $U = 15$ m/s to prevent possible damage to the hardware. Even though the

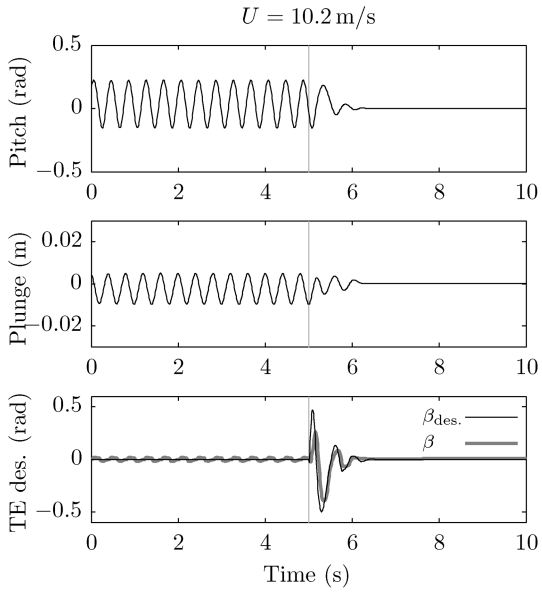

Fig. 2 Limit-cycle oscillation test at $U = 10.2$ m/s. The limit-cycle oscillations are allowed to develop with the controller turned off, then at time $t = 5$ s the controller is enabled.

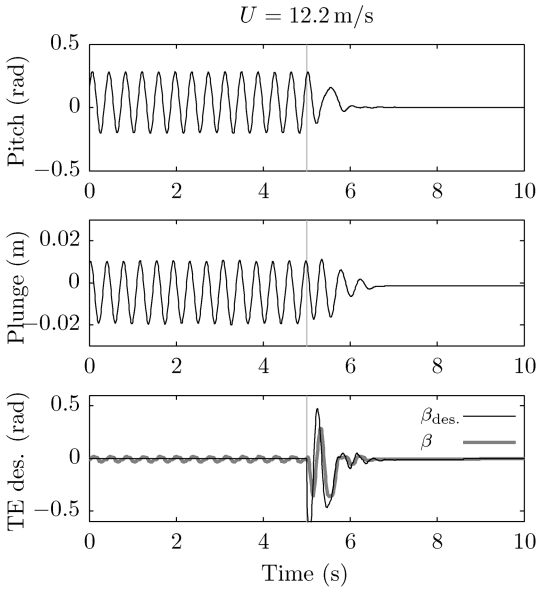

Fig. 3 Limit-cycle oscillation test at $U = 12.2$ m/s. The limit-cycle oscillations are allowed to develop with the controller turned off, then at time $t = 5$ s the controller is enabled.

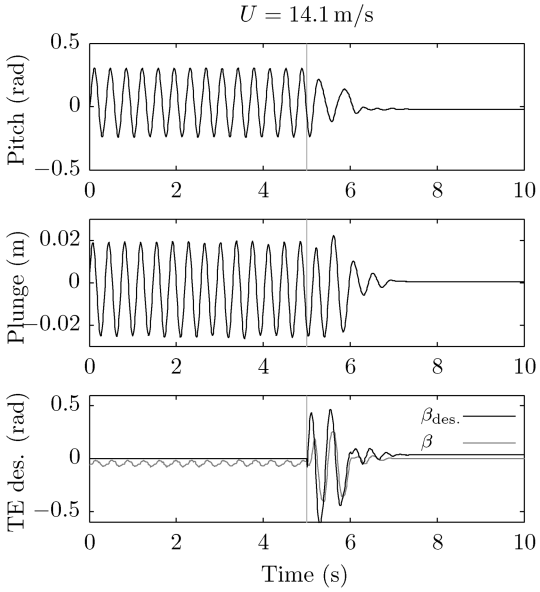

Fig. 4 Limit-cycle oscillation test at $U = 14.1$ m/s. The limit-cycle oscillations are allowed to develop with the controller turned off, then at time $t = 5$ s the controller is enabled.

controller was unable to be tested above $U = 15$ m/s, the successful verification of the controller gains and performance value shows that the controlled system is theoretically stable with an $\mathcal{H}_2$ norm less than $\sqrt{108.5}$ across the airspeed design range.

The ability of the controller to suppress limit-cycle oscillations was tested at several different airspeeds. Initially, the controller was off, allowing the limit-cycle oscillations to develop, then at $t = 5$ s the controller was enabled. Results for $U = 10.2$, 12.2, and 14.1 m/s are shown in Figs. 2–4, respectively. As can be seen, in all cases, once the controller is enabled at $t = 5$ s, the limit-cycle oscillations are suppressed and the system settles after approximately 1 s, while placing only moderate demands of frequency and amplitude on the trailing-edge control surface. This is significantly better than previous experimental attempts, such as in Platanitis and Strganac [4], where the adaptive controller heavily saturated the control surfaces in order to suppress the limit-cycle oscillations over a longer duration.

VI. Conclusions

Through the inclusion of the servo motor dynamics in the aeroelastic model, a controller effective in suppressing limit-cycle oscillations can be synthesized despite the torsional stiffness nonlinearity, as has been shown.

Using an LPV formulation for the aeroelastic system, it has been shown that an LPV controller can be synthesized such that it autoschedules with airspeed and that this controller effectively suppresses limit-cycle oscillations over a range of airspeeds.

Acknowledgments

Research undertaken for this Note has been assisted with a grant from the Sir Ross and Sir Keith Smith Fund (Smith Fund). The support is acknowledged and greatly appreciated. The Smith Fund, by providing funding for this project, does not verify the accuracy of any findings or any representations contained in it. Any reliance on the findings in any written report or information provided to you should be based solely on your own assessment and conclusions. The Smith Fund does not accept any responsibility of liability from any person, company, or entity that may have relied on any written report or representations contained in this Note if that person, company, or entity suffers any loss (financial or otherwise) as a result.

References

[1] Mukhopadhyay, V., "Historical Perspective on Analysis and Control of Aeroelastic Responses," *Journal of Guidance, Control, and Dynamics*, Vol. 26, No. 5, 2003, pp. 673–684. doi:10.2514/2.5108

[2] Waszak, M., "Modeling the Benchmark Active Control Technology Wind-Tunnel Model for Application to Flutter Suppression," AIAA Atmospheric Flight Mechanics Conference, AIAA Paper 96-3437, San Diego, CA, 1996.

[3] Strganac, T. W., Ko, J., and Thompson, D. E., "Identification and Control of Limit Cycle Oscillations in Aeroelastic Systems," *Journal of Guidance, Control, and Dynamics*, Vol. 23, No. 6, 2000, pp. 1127–1133. doi:10.2514/2.4664

[4] Platanitis, G., and Strganac, T. W., "Control of a Nonlinear Wing Section Using Leading- and Trailing-Edge Surfaces," *Journal of Guidance, Control, and Dynamics*, Vol. 27, No. 1, 2004, pp. 52–58. doi:10.2514/1.9284

[5] Platanitis, G., and Strganac, T. W., "Suppression of Control Reversal Using Leading- and Trailing-Edge Control Surfaces," *Journal of Guidance, Control, and Dynamics*, Vol. 28, No. 3, 2005, pp. 452–460. doi:10.2514/1.6692

[6] Feron, E., Balakrishnan, V., Boyd, S., and Ghaoui, L. E., "Numerical Methods for $\mathcal{H}_2$ Related Problems," *Proceedings of the American Control Conference*, American Automatic Control Council, Evanston, IL, 1992, pp. 2921–2922.

[7] Xie, W., "$\mathcal{H}_2$ Gain Scheduled State Feedback for LPV System with New LMI Formulation," *Control Theory and Applications*, Vol. 152, No. 6, 2005, pp. 693–697. doi:10.1049/ip-cta:20050052

[8] Scherer, C. W., "Robust Mixed Control and Linear Parameter-Varying Control with Full Block Scalings," *Advances in Linear Matrix Inequality Methods in Control*, edited by L. El Ghaoui, and S.-I. Niculescu, Society for Industrial and Applied Mathematics, Philadelphia, 2000, Chap. 10, pp. 187–208.

[9] Prime, Z., Cazzolato, B., and Doolan, C., "A Mixed $\mathcal{H}_2/\mathcal{H}_\infty$ Scheduling Control Scheme for a Two-Degree-of-Freedom Aeroelastic System Under Varying Airspeed and Gust Conditions," *AIAA Guidance, Navigation, and Control Conference*, Honolulu, HI, AIAA Paper 2008-6787, 18–21 Aug. 2008.

[10] Löfberg, J., "Yalmip : A Toolbox for Modeling and Optimization in MATLAB," *IEEE International Symposium on Computer Aided Control Systems Design*, Inst. of Electrical and Electronics Engineers, Piscataway, NJ, 2004, pp. 284–289. doi:10.1109/CACSD.2004.1393890

[11] Toh, K. C., Todd, M. J., and Tutuncu, R. H., "SDPT3—A MATLAB Software Package for Semidefinite Programming," *Optimization Methods and Software*, Vol. 11, Nos. 1–4, 1999, pp. 545–581. doi:10.1080/10556789908805762